Neural Computing and Applications (2023) 35:7315–7338
https://doi.org/10.1007/s00521-021-06709-w

S.I. : NEURO, FUZZY AND THEIR HYBRIDIZATION

Brain tumor segmentation using extended Weiner and Laplacian lion optimization algorithm with fuzzy weighted k-mean embedding linear discriminant analysis

Surbhi Vijh[1] · Hari Mohan Pandey[2] · Prashant Gaurav[3]

Received: 3 June 2021 / Accepted: 27 October 2021 / Published online: 8 January 2022

Abstract

This paper presents an efficient skull stripping method to improve the decision-making process. Extended Weiner filtering (EWF) is used for removing the noise and enhancing the quality of images. Further, laplacian lion optimization algorithm (LXLOA) is implemented. LXLOA utilizes the Otsu's and Tsallis entropy fitness function to determine an optimal solution. The implemented LXLOA provides a threshold value required for performing the segmentation on the brain MRI images. The extracted features are selected using fuzzy weighted k-means embedding LDA (linear discriminant analysis) method for improving training of the classification model. The proposed LXLOA is extensively tested on standard benchmark functions CEC 2017 and outperforms the existing state-of-the-art algorithm. Rigorous statistical analysis is conducted to determine the statistical significance. Three-fold performance comparison is performed by considering (a) the quality of the segmented image; (b) accuracy, sensitivity, and specificity; and (c) computational cost of convergence for finding an optimal solution. Result reveals that LXLOA gives promising results and demonstrate effective outcomes on the standard quality measures (a) accuracy (97.37%); (b) sensitivity (85.8%); (c) specificity (90%); and (d) precision (91.92%).

Keywords Brain tumor images · Extended Weiner filter · Laplacian lion optimization algorithm · Fuzzy weighted k-means embedding LDA · Classification

Abbreviations

EWF	Extended Weiner filter
LXLOA	Laplacian lion optimization algorithm
WOA	Whale optimization algorithm
APSO	Adaptive particle swarm optimization
DE	Differential evolution
LOA	Lion optimization algorithm
ACSA	Adaptive cuckoo search algorithm
PSO	Particle swarm optimization
GWO	Grey wolf optimization
CSA	Cuckoo search algorithm
CSO	Cat swarm optimization
CNN	Convolutional neural network
IBSR	Brain segmentation repository
MRI	Magnetic resonance imaging
CT	Computed tomography
PSRN	Peak signal-to-noise ratio
SSIM	Structural similarity index measure
RMSE	Root mean square error
SVM	Support vector machine
ANN	Artificial neural network
LDA	Linear discriminant analysis
FKM	Fuzzy weighted K-mean
WHO	World Health Organization
3-D	3-Dimensional
CT	Computed tomography
LB	Lower bound
UB	Upper bound
DIM	Dimension

Surbhi Vijh and Hari Mohan Pandey equally contributed to this work.

✉ Hari Mohan Pandey
Pandeyh@edgehill.ac.uk

Surbhi Vijh
surbhivijh428@gmail.com

Prashant Gaurav
prashantgaurav36@gmail.com

[1] Department of Information Technology, KIET Group of Institution, Ghaziabad, India

[2] Department of Computer Science, Edge Hill University, Ormskirk, Lancashire, England

[3] V R Techniche Consultants Pvt Ltd, Noida, India

GLCM	Grey level co-occurrence matrices
GLDM	Grey level difference matrix
CEC	Congress on evolutionary computation
$K(x, y)$	Filter
U(d, h)	Fourier transform of PSF (point spread function)
$P_s(d, h)$	Power spectrum of the processed signal process
$P_n(d, h)$	Power spectrum of processed noise
SI	Dispersion index
σ	Standard deviation
μ	Mean
EWF (x,y)	Extended wiener filter
M_{final}	Fitness value
α,β	Random values ranging from 0 to 1
M_{Otsu}	Otsu's function
$M_{Tsallisentropy}$	Tsallis entropy
l_i	Laplacian distributed random ''number
w	Location
q	Scale parameter
u_i,v_i	Distributed random numbers having range [0, 1]
New_Cub$_M$	Offspring (New cube)
x^i_{male}	Male in pride
x^i_{female}	Female in pride
U	Universal function
K$_{(x,y)}$	Factor of features
s_{xk}	Membership function showing the fuzzy cluster
Wfb	Fuzzy weighted k-means
y_{ie}	Factor
c_{ke}	Weighted mean
f_{ek}	Weight of feature e for cluster k.
m_{xy}	Weighted mean
g_y	Sample of data belonging to y
n_x	Count of data points reside in x
g	Relative distance from the cluster
m	Fuzzifier function

1 Introduction

The automatic computer-aided diagnostic procedures are unfolding medical imaging research to explore and visualize tremendously emerging patterns [1, 2]. The growing standardization in clinical decision-making advances the process and increases the patient's survival rate at an early stage. Computer vision and pattern recognition help the radiologist, physician, pathologist, and experts in the contribution of advanced techniques for the treatment of patients [3, 4]. Medical imaging segmentation is an essential and challenging task for improving the decision-making process's performance [5–7].

In their reports, WHO (World Health Organization) and American Brain Tumor Association have classified brain tumor as benign and malignant tumor types. Grading of these tumor types can be done on a scale from grade I to grade IV. However, National Brain Tumor Society report states that over 87,000 people will be diagnosed with a primary brain tumor in 2020 in the United States. Hence, this estimation states that there will be 61,430 brain tumor benign cases and 25,800 brain tumor malignant cases.

Image processing plays a crucial role in enhancing prominent finding effectiveness and identifying the patterns [8, 9]. The multidimensional image can be generated using two modalities for radiological medical imaging applications such as computed tomography (CT) and magnetic resonance imaging (MRI) [10]. The most preferred non-invasive modality for acquiring human neural activity is MRI due to high resolution, least ionizing radiation, and soft tissue capabilities [11]. Generally, the different MRI images are utilized for diagnosis purposes, including T1- weighted MRI, Flair with contrast enhancement, Flair and T2-weighted MRI [12] as shown in Fig. 1.

The intelligent detection system helps experts, radiologists, and physicians to decide the uncertainties present in neoplasm. Patel et al. [13] showed the study of different segmentation techniques such (a) thresholding [14] (b) region-based segmentation [15] (c) edge-based segmentation (d) fuzzy c-mean clustering method [16] for medical imaging.

Metaheuristics hybridization is growing exponentially by developing a fusion of two different search operators. The proposed LXLOA algorithm is derived from the merits of the laplacian crossover and lion optimization algorithm. LXLOA is implemented for segmentation and contributes to the skull stripping process. LXLOA algorithm provides a new optimal solution in mating phase by producing new offspring. LXLOA selects the best male agent (high fitness value) to mutate with female lion for generating a new cub. Laplacian operator explores best probable male lion to replace with worst performing lion. Thus, the best solution is obtained for efficient segmentation of brain MRI images.

The key contributions are highlighted as follows:

(i) An intelligent brain tumor detection and diagnosis model is proposed for computer-aided diagnosis systems. Extended Weiner filtering is applied for improving the intensity of images. Further, LXLOA algorithm is based on Otsu's and Tsallis

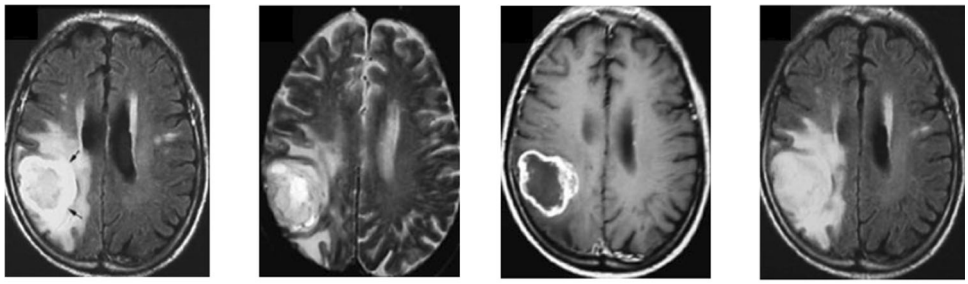

(a) (b) (c) (d)

Fig. 1 Representative of **a** T1-Weighted MRI **b** Flair **c** Flair with Contrast Enhancement **d** T2-Weighted MRI

entropy function to obtain the threshold value and perform segmentation. This process improves the convergence speed. Thus, efficient skull stripping of brain MRI is designed.

(ii) A fuzzy weighted k-means embedding linear discriminant analysis algorithm is implemented for the prominent selection of optimized features subset. The artificial neural network (ANN) is used for classification purposes.

(iii) Extensive computer simulations and testing are conducted on benchmark functions to determine the efficiency and effectiveness of the proposed method. Moreover, statistical tests are performed for determining the performance significance of acquired results. Further, three-fold comparison is performed as follows:

  (a) Firstly, the quality of the segmented image is measured using three quality metrics: (a) fitness value; (b) peak signal-to-noise ratio (PSRN) value; and (c) structural similarity index measure (SSIM) value.
  (b) Secondly, the classification method is trained with acquired selected features from the fuzzy weighted k-means embedding LDA to compute accuracy, sensitivity, and specificity.
  (c) Thirdly, the effectiveness of the LXLOA is evaluated in terms of the computational cost of convergence for finding an optimal solution.

The performance of the proposed LXLOA (Algorithm 1) is compared against the state-of-the-art metaheuristic algorithms such as DE [17], WOA [18], PSO [19], LOA [20], ACSA [21]. The performance of algorithm depends on the selection of its parameter. These algorithms belong to the family of swarm intelligence algorithms. These are nature-inspired metaheuristic algorithm, and they get converged to the optimal global solution. These algorithms approach towards optimal solution but cannot guarantee it. The rationale behind selecting these algorithms are as follows: (a) DE algorithm holds good exploration ability for optimization problem.(b) WOA [22] maintains a good balance between exploration and exploitation stage and avoids the premature convergence. (c) PSO iteratively updates the position via a swarm of particles for determining the optimal solution. (d) LOA adopts different strategies depending upon the social organization and behavior of lions to find the optimal solution. (e) ACSA's functionalities are based on breeding of cuckoo birds and works on exponentially increasing switching parameters to provide improved solution.

The paper is structured in different sections as follows: Sect. 2 presents related work and standard lion optimization algorithm; Sect. 3 discusses the proposed methodology; Sect. 4 describes experimental setup, results, and discussion; and Sect. 5 shows the conclusions and future research directions.

2 Related work

Bio-inspired algorithms and swarm intelligence are nature-inspired techniques that help to solve real optimization problems [23]. Various metaheuristic algorithms are applied in image segmentation to obtain refined results and effective performance [24]. Few popular optimization algorithms are artificial bee colony (ABC) [25–28], particle swarm optimization (PSO) [29], whale optimization algorithm (WOA) [30], genetic algorithm (GA) [31], adaptive particle swarm optimization [32], cuckoo search algorithm [33, 34], grey wolf optimization [35], cat swarm optimization [36], and lion optimization algorithm [37]. These optimization algorithms provide the optimal global solution for the selected set of features through exploitation and exploration [34, 38, 39]. A comparative analysis of different existing algorithms is summarized and presented in Table 1.

Manic et al. [48] stated the approach for segmenting the grayscale image based on firefly optimization algorithm using multi-level thresholding. The Kapur's and Tsallis functions were selected for determining the optimal

Table 1 Comparative analysis of existing algorithms with respect to brain MRI dataset, approaches used, and performance

Author	Dataset	Approach	Performance
Wang et al. [40]	BRATS 2017	Anisotropic and Cascaded CNN model	–
Kumar et al. [41]	T1 weighted MRI -55 patient	PCA –ANN, Gradient vector flow boundary	95.37%
Sharma et al. [42]	T1 weighted MRI	Global thresholding, Post-processing using anisotropic diffusion filtering, DE + ANN	94.3%
El Abbadi et al. [43]	65 MRI weighted brain image	Probabilistic neural network	98%
Lashkari et al. [44]	T1 & T2 weighted MRI—210 case	Histogram equalization, MLP model- ANN	98%
Vijh et. al [45]	T1 weighted MRI—61 sample case	Hybrid of Otsu and Adaptive particle swarm optimization	98%
Chao et al. [46]	MNIST	CaRENets	Overall (0.925) accuracy
Zhao et al. [47]	2013 benchmark BRATS data	Patch-wise Convolutional neural network	Overall (0.81) Accuracy

threshold value for segmenting the images. Thus, the simulation results were evaluated and tested; the algorithm gave better outcomes on comparative analysis. However, the quality metrics of the image were determined using parameters like (a) peak-signal-to-noise-ratio (PSNR); (b) root mean square error (RMSE); (c) structural similarity index matrix (SSIM); and (d) normalized absolute error.

Soleimani et al. [49] implemented the ABC optimization algorithm for segmentation of brain tumor to perform diagnosis and improve the model's accuracy. Jafari et al. [50] proposed a hybrid method for the detection and prognosis of brain tumor MRI imaging. The simulated steps were performed utilizing thresholding, post-processing fast Fourier transform, feature selection through the genetic algorithm, classification using a support vector machine. The performance measures were computed by determining the accuracy of 83.22%.

Yin et al. [51] proposed a novel approach by applying the multilevel thresholding using differential evolution (DE) optimization algorithm for producing a segmented image. Pugalenthi et al. [52] presented the method in which preprocessing is performed by applying social group optimization and fuzzy Tsallis thresholding for improving the intensity of the brain tumor section so that the region can adequately be segmented. The features were extracted by considering the GLCM technique and analyzing the classification using the SVM-RBF kernel for benign and malignant tumors. The evaluated accuracy for the model was estimated at 94% on the MRI brain image dataset.

Natarajan et al. [53] stated the techniques for efficient brain tumor segmentation by implementing preprocessing, segmentation, and post-processing on MRI images. Manogaran et al. [54] presented the approach for identifying the abnormalities present in brain image using orthogonal gamma distribution for determining the under and over segment region on 994 MRI brain images of 30 patients. The wavelet and GLCM based features are extracted from the segmented image, and morphological-based operation was applied for the post-processing of brain MRI tumor image. Further, the image quality was measured using quality metrics as PSNR and MSE parameters.

Havaei et al. [55] implemented the convolutional neural network (CNN) for automatic brain tumor segmentation on the BRATS (2013) benchmark dataset. Bansal et al. [56] proposed multilayer perceptron architecture using lion optimization algorithm (MLP-LOA) for classification purpose. The different stages of the LOA were implemented for determining the optimal solution. The MLP-LOA algorithm efficiency was evaluated by comparing with different existing classification algorithm.

2.1 Lion optimization algorithm

Swarm intelligence and evolutionally computational-based metaheuristics algorithms have been successfully implemented for solving various real-time complex optimization problem. Lion optimization algorithm (LOA) [57] is a popular metaheuristics algorithm inspired by the social organization and behavior of the lion. The formation of initial population is consisting of randomly generated solutions. The social organization of lions is categorized namely as nomads and residents, respectively. Resident lion also referred to pride consisting majority (75–90%) of female lion and remaining as male lion. The pride territory members contain the best-visited position in the region. In LOA, the different procedures and strategies are followed by each specific gender to search for optimal solution.

Typically, lion forms the coordinated group to encircle and hunt the prey. Furthermore, in the region of pride territory, randomly some females are selected for hunting, however the remaining female moves in different location of territory. In pride, each male resident lion roams in its own territory. During roaming, resident male lion updates their position if lion reaches a new position which is finer than the current position. The roaming behavior of lion enables strong local search and provides improved solution. Mating process increments the growth in population of lion and helps in exchanging information among the members in pride. In each pride, $\% X_{mt}$ of female lions intimate with one or more randomly selected male resident lion from the same pride to produce offspring [58]. However, the nomad female lion mates with one of the randomly selected male among the nomads. During mating, the produced offspring is randomly chosen as female and male. Further, defense operation of lion is performed to retain the best male lions as solution playing a vital role in LOA. So, the defense operation is two-stage process: (i) defense against newly developed mature resident male's lion in pride; and (ii) defense against nomad males. The migration behavior of lion is inspired by the switch lifestyle, where lions exchange from one pride to another pride territory. The migration characteristic helps in improving the diversity of pride and exchanging information. Thus, lion optimization algorithm introduces various operators that help in achieving the optimal solutions.

3 Material and methods

This section shade light on the proposed methodology for the development of intelligent brain tumor detection. The working of the proposed system is divided into six stages are discussed in subsections as follows: (a) brain MRI acquisition; (b) skull stripping of brain MRI (i) image preprocessing using proposed extended Weiner filtering; (ii) image segmentation using proposed LXLOA algorithm; (iii) morphological mathematical operations; and (iv) eliminating cerebral tissue); (c) applying anisotropic diffusion; (d) feature extraction; (e) feature selection; and (f) classification. The flow process of proposed methodology is depicted in Fig. 2.

Series of simulations have been conducted to evaluate the performance of the proposed LXLOA algorithm. All simulations were performed on Intel core i7 with 2.2 GHz speed, 16 GB RAM, NVIDIA Geforce GTX1080 ti 4 GB, and Windows 10 operating system. MATLAB 2018b was used for implementing the proposed algorithm. Extensive parameters tuning was performed for developing the robust simulation model for the implementation of the proposed system (see Fig. 2). LXLOA was implemented using the parameters presented in Table 2, while Table 3 shows the ANN's parameters selected for training the network.

3.1 Brain MRI data and normalized image

T1-weighted brain MRI data consist of 250 samples attained from IBSR (brain segmentation repository) (IBSR), and 150 sample images of MS free data are collected from the Laboratory of eHealth at the University of Cyprus [59] and Institute of neurology and genetics, at Nicosia Cyprus. The obtained sample images are normalized for improving the intensity of images so that effective segmentation and pattern recognition can be visualized.

3.2 Skull stripping

Skull stripping plays an essential role in brain MRI medical imaging for enhancing the clinical research and decision-making process [60, 61]. It is a crucial preprocessing phase for removing cerebral tissue and improving the analysis of brain magnetic resonance images. In the proposed work, the automatic skull stripped algorithm is developed by contributing the two major processes (i) applying extended wiener filtering technique to enhance the quality of images (ii) LXLOA algorithm to obtain fitness value for segmentation of brain MRI image.

3.2.1 Extended Weiner filtering (EWF)

After normalizing the image, the statistical approach of proposed extended Weiner filtering (EWF) is applied to remove noise and enhance brain MRI quality. The mathematical equation of Weiner filtering [62] in Fourier transform is shown in Eq. (1). EWF utilizes the dispersion index which ensures whether the set of obtained occurrences are dispersed or clustered. Dispersion index (SI) is the ratio of variance and mean for noise estimation as shown in Eq. (2). The filter reduces the mean squared error criteria and smoothens the image. The mathematical formation of extended Weiner filtering is depicted in Eq. (3).

$$K(x,y) = \frac{U*(d,h)P_s(d,h)}{|U(d,h)|^2 P_s(d,h) + P_n(d,h)} \tag{1}$$

$$\mathrm{SI} = \frac{\sigma^2}{\mu} \tag{2}$$

$$\mathrm{EWF}(x,y) = K(x,y) + \frac{\mathrm{SI} - \sigma^2}{\mathrm{SI}} K(x,y) \tag{3}$$

Here, $K(x,y)$ represents the filter, image U(d, h) shows the Fourier transform of PSF (point spread function), $P_s(d,h)$ is the power spectrum of the processed signal process, $P_n(d,h)$ is the power spectrum of processed noise. *SI*

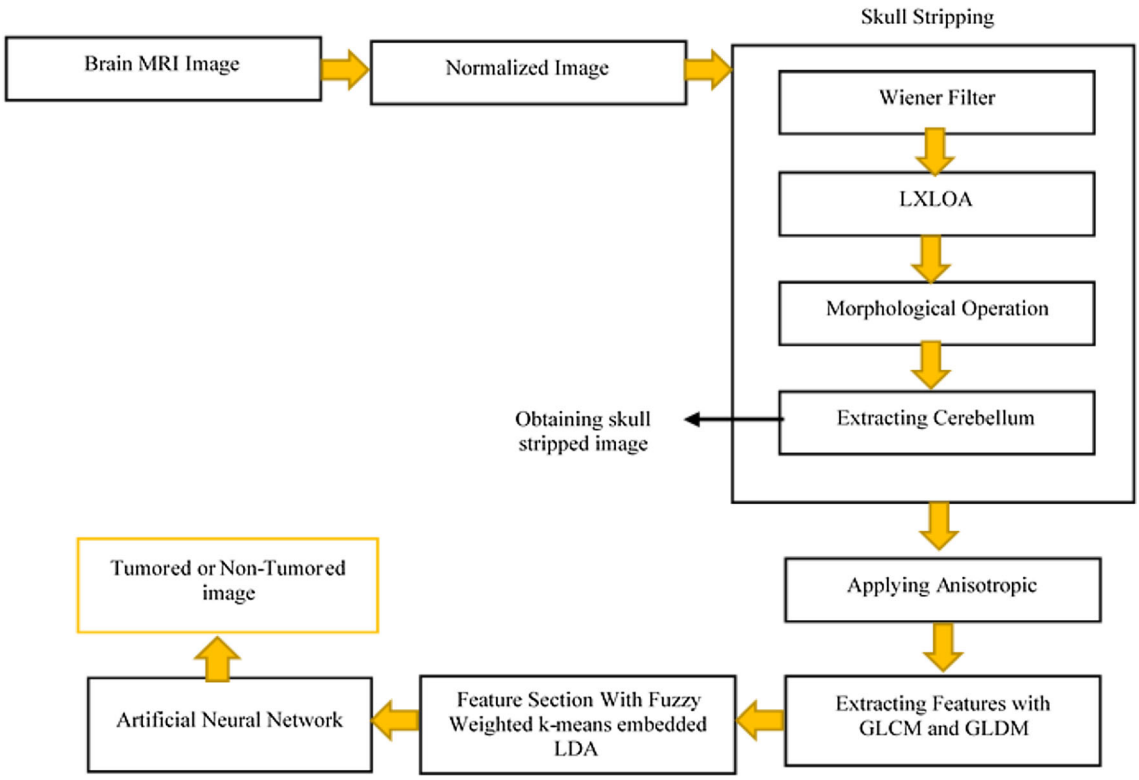

Fig. 2 Flow daigram of the proposed methodology

Shows the dispersion index, σ and μ shows the standard deviation and mean, EWF (x,y) is extended wiener filter.

3.2.2 Laplacian lion optimization algorithm

Image segmentation is a necessary and challenging task for image analysis and diagnosis of disease. The fitness values are generated with combination of otsu's function and tsallis entropy as shown in Eq. (4). Fitness value is considered as optimal threshold value for segmentation. In LXLOA algorithm, mating process increments the growth in population of lion and helps in exchanging information among the members in pride. In each pride, % X_{mt} of female lions intimate with one or more resident male lion having high fitness value (best agent) from the same pride to produce the offspring. However, the nomad female lion mates with one of the best male agent among the nomads. A mutation with probability is applied on each gene of generated offspring for enhancing the inherited characteristics of new cub and balancing the computation cost. The laplacian crossover operator [63] is referred to as linear combination of parents for generating pair of new best

Table 2 Parameters and values

Parameter	Value
Number of prides	4
Sex ratio	0.8
Percent of nomad lions	0.2
Mating probability	0.3
Roaming percent	0.2
Immigrate rate	0.4
Mutation probability	0.2
Population size	200

Table 3 Parameters and values used in the ANN

Parameters	Values
Number of layer	3
Learning rate	0.1
Activation function	tanh, sigmoid
Optimizer	Adam
Batch size	2
Epochs	50
Loss	Categorical crossentropy
Validation split	0.8/0.2
Training and testing set	7:3

offspring as depicted in Eq. (5). The offspring are produced using Eqs. (6) and (7) respectively. The parameters and their respective values are presented in Table 2. The parameters are selected on the basis of permutation and combination and best values are considered. The detailed proposed LXLOA is depicted in Algorithm 1.

$$M_{\text{final}} = \alpha M_{\text{Otsu}} + \beta M_{\text{Tsallisentropy}} \tag{4}$$

$$l_i = \begin{cases} w - q\log_e(u_i), v_i \leq \dfrac{1}{2} \\ w + q\log_e(u_i), v_i < \dfrac{1}{2} \end{cases} \tag{5}$$

$$\text{New\_Cub}_M = x^i_{\text{male}} + l_i\left|x^i_{\text{male}} - x^i_{\text{female}}\right| \tag{6}$$

$$\text{New\_Cub}_M s = x^i_{\text{female}} + l_i\left|x^i_{\text{male}} - x^i_{\text{female}}\right| \tag{7}$$

Here,M_{final} is the fitness value,α, β are the random values ranging from 0 to 1, M_{Otsu} and $M_{Tsallisentropy}$ represents the Otsu's function and Tsallis entropy.l_i shows the laplacian distributed random number, w and q (q > 0) represents the location and scale parameters. (u_i) and(v_i) are the two distributed random numbers having range [0,1].New_Cub$_M$ and New_Cub$_M s$ are obtained offspring. If produced offspring doesn't belong to search space, in that case, New_cub^i is kept to as random number in interval $[New\_cub^i_{low}, New\_cub^i_{up}]$, x^i_{male} represents the male in pride, x^i_{female} shows the female in pride.

Algorithm 1 presents the proposed laplacian lion optimization algorithm (LXLOA). It takes image as an input and producsed a final processed image for feature extraction.

Algorithm 1: Laplacian Lion Optimization Algorithm (LXLOA)

Term used: *L*: Lion, *F*: Resident rate of lion, *RP*: Roaming percentage of pride, X_{mt}: Mutation probability, *IR*: immigration rate of LOA, f_{final}: Best optimal value, *O*: extracted features , *i*: no of iteration, *P*: population generated randomly, *No_Iteration*: maximum number of iterations, *Female_Lion*: Random female lion to go on hunting, *R_Female_Lion*: Remaining female lion that move toward the best visited from pride territory, *IRFL*: Immigrate resident female lion, New_Cub_C: New cubs are generated after crossover operation, New_Cub_M: New cubs are generated after mutation operation, New_Cub_{upp}: New cub after replacing worst performing lion in pride, New_Cub_{upn}: New cub after replacing worst performing lion in nomade, *FV*: Fitness Value, $Image_{bestvalue}$:The optimal best value for image is generated at f_{final}

Input: Image E(x,y).

Output: Final processed image for feature extraction (O).

Begin
  Set P ← Generation of random population upto L of lion over the solution of image.
  Perform pass the generated values with FV using Eq. (4).
  While i < =No_Iteration *do*
    For begin nomad and pride lion *do.*
      Set L ← Select L of nomad lion from P.
      Set (1-L) ←Remaining (1-L) forms the pride territory.
      For each pride do
        Set F ← Rate of resident population as female and remaining as males.
    End For
    For each pride *do*
      Set Female_Lion ← Selection of random female lion to go on hunting.
      Set R_Female_Lion ← Move towards the best explored from pride territory.
      Set RP ← Randomly selected for each resident lion.
      Apply laplacian crossover over best selected lion (using Eq. (6) and (7))
      Set New_Cub_C ← R_Female_Lions intimate with resident male lion.
      Set New_Cub_{upp} ← New_Cub (Replacing worst performing lion in pride).
    End For
    For each nomad lion *do*
      New_Cub_M ← Nomad female lion mutate with one of the best male agent.
      Apply laplacian crossover over best selected lion.
      New_Cub_{upn} ← Replaces the worst performing lion in nomad.
      Nomad male randomly attacks the prides.
    End For
    For each lion pride *do*
      Set IRFL ← IRFL from territory and becomes nomad lion.
    End For
    Perform migratory operation using steps (29) – (31).
    Select (R_Female_Lion) ← R_Female_Lion with the lower FV in pride.
    Set Nomad ← R_Female_Lion.
    Set $Pride_{update}$ ← Nomade female with the best FV.
    Balance lion's population equilibrium at the end of each iteration.
    Set FV ← Update FV.
    Set i ← i + 1.
  End While
  Generate $Image_{bestvalue}$ ← Optimal best value for image is generated f_{final}.
  Perform morphologyical and skull stripping operations on segmented image (O).
End.

Step-by-step working of Algorithm-1 Algorithm 1 presents the proposed LXLOA. It accepts image E(x, y) as inputs and produces final processed image for feature extraction (O). Algorithm 1 begins at step-2 by generating a random population (P) up to L of lion from the input images E(x, y). Step-3 is responsible for evaluating fitness value by combining both Otsu's function and Tsallis entropy as indicated in Eq. (4). The main functionality of Algorithm 1 is in a while loop which runs from steps 4–35. The while loop at step-4 runs until it reaches the maximum number of iteratirons (No_Iteration). From steps 5–10 a for loop is implemented which is responsible for selection of nomad pride and pride territory. At step-6, lion (L) is selected as nomad lion from the total population (P), while the remaining (1-L) forms the pride territory as indicated at step-7. At steps 8–9, a for loop is implemented for each pride to set the percent of F (resident rate of lion) population as female and remaining as males. This rate percent gets inversed in the nomad lions. Another for loop is implemented from steps 11–18. This for loop deals with female lions is selected randomly for hunting (step 12) and exploring the pride territory (step 13). After that, in pride, the roaming percentage (RP) of pride territory are randomly selected for each resident lion as shown at step 14. Steps 15–17 are given to present the crossover operation and replacement of the worst-performing lion in pride. We have used Eqs. (6–7) to perform crossover operation. Mutation operation is performed from steps 19–24. Here, nomad female lion mutates with one of the best male agents among the nomads to produce new offspring ($\text{New\_Cub}_{\text{M}}$) as shown in step 20. Then, apply laplacian crossover over the best-selected lion (step 21). At step 22, new cub ($\text{New\_Cub}_{\text{upn}}$) replaces the worst-performing lion in nomad. And then, nomad male randomly attacks the pride (step 23). A for loop at steps 25–27 is presented for the percentage of immigrates resident female lion (IRFL). Here, IRFL indicates the percentage of female lion immigrates from territory and becomes nomad lion. Migration operation is performed from steps 29–31. It is performed by selecting the resident female lion (R_Female_Lion) having the lower fitness value in pride (step 29) and converting them to nomad (step 30). Further, the vacant places in each pride are fulfilled, by migrating or distributing the nomad female having best fitness value as indicated in step 31. Lion's population equilibrium is balanced at the end of each iteration, so, considering the maximum population of gender in nomad category, the lions having least fitness value are removed (step 32). Thus, the control is maintained on number of live lions. At this stage, update the fitness value as shown in step 33 and move to the next iteration (step 34). The while loop terminates at step 35. Step 36 and 37 are respectively for generation the optimal best value for images and to perform morphological and skull stripping operations on segmented image.

3.2.3 Mathematical morphological operations and skull stripping

The mathematical morphological operations are post-processing functionalities performed on images using the structuring element. The transformation operations are implemented on segmented images using erosion and dilation to perform the analysis.

The skull stripping is achieved by eliminating the extracerebral tissue and visualizing the extracted mask for conducting exploration and region of interest.

3.3 Anisotropic diffusion filtering and feature extraction

It is implemented for denoising purpose, i.e., removing the noise and enhancing the contrast as well intensity among the different brain MRI sections. The filtering maintains the balance for existing different levels of noise in the image.

It is crucial for identifying the pattern and determining the texture, statistical analysis. Grey level co-occurrence matrices (GLCM) [64–66] and grey level difference matrix (GLDM) are the second-order statistical measures that are applied to extract the 23 features from brain MRI segmented image. There is general applicability of grey level-based texture features spatial dependencies or relationship in image classification. The 23 extracted statistical features in the proposed work namely are contrast, entropy, difference entropy, autocorrelation, homogeneity, cluster prominence, inverse difference, information measure of correlation 1 (Imc 1), cluster shade, information measure of correlation 2 (Imc 2), sum entropy, sum variance, sum of square variance, sum average, horizontal weighted sum, maximum probability, grid weighted, diagonal weighted sum, vertical weighted sum, energy, correlation, dissimilarity.

3.4 Feature selection

It is achieved using fuzzy weighted k-means (FKM) embedded LDA (Algorithm 2) for determining the

optimized set of features. The FKM embedding LDA is applied for providing the solution to the multidimensional pattern recognition problem. The mathematical formulation of fuzzy weighted k-means is expressed through Eqs. (8), (9,) and (10), respectively. The calculation of the weighted mean is performed using Eq. (11). The modification in the membership matrix and Bayes rule of LDA is depicted in Eq. (12).

$$U = [K_{(x,y)}]\ 1 \leq x \leq e,\ 1 \leq y \leq e \tag{8}$$

$$\sum_{k=0}^{n} k_x y = 1, y = 1, 2, 3 \ldots n \tag{9}$$

$$\mathrm{Wfb} = \sum_{k=1}^{k} \sum_{i \in 1} \sum_{(e=1)}^{m} s_{xk}^{\alpha} f_{ek}^{\beta} |y_{ie} - c_{ke}|^2 \tag{10}$$

Here, U represents the universal function,$K_{(\mathrm{x,y})}$ shows the factor of features, s_{xk} is the membership function showing the fuzzy cluster, Wfb is the fuzzy weighted k-means, y_{ie} and c_{ke} represents factor and unsupervised weighted mean, f_{ek} shows the weight of feature e for cluster k.

$$m_{\mathrm{xy}} = \frac{\sum_{x=1}^{n} u_{\mathrm{xy}}^{m} \sum_{x=1}^{n} s_{\mathrm{xk}}^{m} \sum_{x=1}^{n} s_{\mathrm{xk}}^{m}}{\sum_{y=1}^{n} s_{\mathrm{xk}}^{m} \sum_{y=1}^{n} s_{\mathrm{xk}}^{m}} \tag{11}$$

$$f_{\mathrm{xy}} = \frac{\left(||g_y - m_{\mathrm{xy}}||^2 - n_x ||m_{\mathrm{xy}} - g||^2 \right)^{\frac{-1}{m-1}}}{\sum_{k}^{c} \left(||x_y - m_{\mathrm{xy}}||^2 - n_x ||m_{\mathrm{xy}} - g||^2 \right)^{\frac{-1}{m-1}}} \tag{12}$$

In Eq. (12), m_{xy} shows the weighted mean,g_y is the sample of data belonging to y, n_x is the count of data points reside in x, g is the relative distance from the cluster, m is the fuzzifier function.

In Algorithm 2, the fuzzy weighted k-means embedding LDA is applied on acquired statistical features for selecting the finest features to obtain precise accuracy. The membership matrix is initialized (Step-1), and the random value [0, 1] is determined (Step-2). A while loop is executed from steps 3–7, considering the average of the square differences between the membership matrixes. Within the while loop, two tasks are accomplished: (a) fuzzy weighted k-means embedding LDA is calculated through Eq. (10) and Eq. (11); and (b) membership matrix (membership functionf_{xy}) is updated using Eq. (12). Finally, the related features are extracted at step-7, and a further classification technique is implemented.

3.5 Artificial neural network

ANN classifies the tumored and non-tumored brain MRI images [67–69]. ANN consists of computational multilayer interconnected neurons stimulated from biological neural networks to predict outputs based on specific inputs for training the network. The backpropagation neural network approach is a computationally effective method for updating the weights, therefore the backpropagation architecture is used. The testing was conducted for identifying the best permutation and combination of parameters that determine the robustness. The parameters considered are as follows: (a) layer: [2–6]; (b) learning rate: [0.01, 0.1, 0.2, 0.4]; (c) batch size: [1–3]; (d) epochs: [10, 20, 30, 35, 40, 45, 50, 60, 70, 80]; (e) activation function: [tanh, sigmoid, relu]; and loss function: [categorical_crossentropy, mean squared error]. Parameters that gave the best results for training the ANN are summarized in Table 3.

Algorithm 2: Fuzzy weighted k-means embedding LDA

Term used: k_{xy} : elements of features, K: Clusters

Input: Extracted Features from GLCM and GLDM technique.

Output: Selected feature for next processing.

1. Initialization of the membership matrix using Eq.8.
2. Generate the random values from [0, 1] such that the elements k_{xy} of K satisfies using Eq.9.
3. *while* (the average of the square differences between the membership matrix):
4. Calculate the fuzzy weighted k-means embedding LDA using Eq.10 an Eq.11.
5. Update the membership matrix with Eq.12.
6. end *while*
7. Selected Feature values extracted.

4 Simulation results, discussion, and analysis

Extensive computer simulations have been performed to evaluate the performance of the proposed algorithm. In the subsections, we present the following: (a) performance comparison on CEC2017 benchmark functions; (b) performance analysis of brain MRI datasets and simulation results are discussed; (c) statistical analysis; (d) discussion on quality matrices; (e) comparison with state-of-the-art algorithms; (f) comparative results and analysis; and (g) discussion of results.

4.1 Performance analysis on CEC 2017 benchmark functions

The proposed algorithm LXLOA is tested on CEC 2017 standard benchmark functions problem [70]. The benchmark functions belong to categories namely, unimodal function (F1-F3), multimodal function (F4-F10), hybrid function (F11-F19), composition function (F20-F29). The mean and best fitness values are computed for showing the effectiveness of proposed algorithm LXLOA against the state-of-the-art algorithms as shown in Table 4. The considered dimensions, number of iterations over 20 runs, and population size are 50, 1000, 200 respectively. Furthermore, observations state that the proposed LXLOA outperforms and provides a significant solution when compared with other metaheuristic techniques.

4.2 Performance analysis on brain MRI datasets

Brain MRI data from two different databases were used during the simulations. 400 sample images were considered for simulations. Algorithm-1 and 2 were implemented respectively to perform: (a) to examine skull stripping and segmentation; and (b) selection of the prominent features. ANN was implemented to process the sample data. Here, sample data is divided into a 7:3 ratio for testing and training purpose. A sample image of IBSR tumored is depicted in Fig. 3, while Fig. 4 represents a sample image of an MS-free dataset on non-tumored MRI.

Tables 5, 6, 7 presents the extracted 18 features obtained by implementing from co-occurrence matrices to analyze the spatial relationship and determine the statistical texture features. 18 features such as cluster prominence, autocorrelation, correlation, contrast, cluster shade, homogeneity, entropy, energy, dissimilarity, sum entropy, sum average, maximum probability, sum of square variance, inverse difference, Imc 2 (information measure of correlation 2), Imc 1, difference variance, and difference entropy are extracted.

On the other hand, Table 8 shows the extracted 5 features using grey level difference matrix for statistical measures for probability density functions. The 5 features are as follows: *grid-weighted sum*, *diagonal-weighted sum*, *vertical-weighted sum*, *horizontal-weighted sum*, and *cluster prominence*. Table 9 presents an optimized feature subset. It presents min, max, and average values of the IBSR and MS free sample images.

4.3 Statistical analysis

Rigorous statistical analysis was performed to determine the statistical performance significance at 95% level of the confidence interval. Equation (13) presents the hypotheses (H_0: null hypothesis and H_A: alternative hypothesis) used to perform the statistical tests.

$$H_0 : \mu_{\mathrm{DE}} = \mu_{\mathrm{WOA}} = \mu_{\mathrm{LION}} = \mu_{\mathrm{LXLOA}} = \mu_{\mathrm{PSO}} = \mu_{\mathrm{ACSA}}$$
$$H_A : \mu_{\mathrm{DE}} \neq \mu_{\mathrm{WOA}} \neq \mu_{\mathrm{LION}} \neq \mu_{\mathrm{LXLOA}} \neq \mu_{\mathrm{PSO}} \neq \mu_{\mathrm{ACSA}} \quad (13)$$

To perform the statistical tests mean and best values of the benchmark functions are used. Sample size 30 has been drawn from each algorithm. We have performed the Kruskal-Wallis test to verify the hypothesis given in Eq. (13).

Table 10 presents the hypothesis test summary of independent samples Kruskal–Wallis test with respect to the best fitness value for across categories of algorithms. We can see p-value is less than 0.05. Hence, H_0 is rejected. It means that one of the other algorithms have shown different performance. We have conducted posthoc test to determine which algorithms have shown different performance.

Figure 5 shows the pairwise comparison of algorithms. It can be noted that each node represents the sample average rank of algorithms. The sample average of the proposed LXLOA (= 43.90) is better than the other algorithms. Total 15 pairs have been formed for pairwise comparison of algorithms. The algorithm pairs LXLOA-PSO, LXLOA-ACSA, LXLOA-WOA, and LXLOA-LION showed significantly better, performance mainly because obtained p-value is less than 0.05. The combinations have not shown significantly better results. This result concludes that LXLOA algorithm is more stable and showing

Table 4 Comparative result analysis on benchmark function suite

Function	Fitness	DE	WOA	LION	PSO	ACSA	LXLOA
f1	Best	1.93E-07	28.22753	2341.614	0.000252	0.564802	5.610218
	Mean	0.005194	15,512,352	2341.614	227.4466	310,474.5	1.416315
f2	Best	5.64E-09	67,881.22	153,623	1.96E-05	1357.624	1.99E-12
	Mean	1.68E-06	85,411.61	183,023	0.679315	1708.912	0.068775
f3	Best	2.61E-07	7.63E-07	3.78E-18	5.17E-24	1.53E-08	8.87E-07
	Mean	9.06E-05	6963.623	0.061275	0.00144	139.2739	1.49E-06
f4	Best	3.13E-06	5.5E-07	5.5E-07	0.000208	0.000208	1.49E-17
	Mean	0.000209	1353.203	2712.742	0.000913	27.06498	7.516757
f5	Best	4.19E-12	0.005024	0.478917	0.000932	0.001033	7.20E-10
	Mean	1.52E-06	0.131142	0.472357	0.009354	0.011977	1.65E-09
f6	Best	1637.905	0.480504	139.496	4.875304	4.884914	1.60E-10
	Mean	1252.855	950.2088	157.136	9.958886	28.96306	0.631596
f7	Best	4.67E-05	0.004733	155.0405	5.850404	5.850499	0.429481
	Mean	0.000313	0.062793	139,675.8	0.9702	0.971456	1.424421
f8	Best	5.07E-08	8.39E-11	9.72E-16	1.47E-32	1.68E-12	5.19E-09
	Mean	0.750191	0.209619	2.9E-15	0.000127	0.004319	5.41E-08
f9	Best	5.18E-13	10,447.23	9693.229	4067.368	4276.313	8.22E-15
	Mean	6.27E-09	10,456.99	9791.229	4067.481	4276.621	2.44E-11
f10	Best	0.388201	28.35728	9,899,686	3.516534	4.08368	4.03E-05
	Mean	0.388252	0.016425	1,762,870	158.5792	158.5795	0.750191
f11	Best	246.3645	5362.274	3783.848	1224.119	1331.365	5.33E-03
	Mean	246.8728	5922.022	37,643.9	1224.408	1342.849	0.024381
f12	Best	0.75255	8.522189	1962.135	2.63669	2.807134	9.48E-07
	Mean	0.695429	5.77E + 08	2807.875	70.28371	11,539,415	0.158039
f13	Best	26.03428	4122.495	3812.395	870.8856	953.3355	7.17E-12
	Mean	28.58031	5391.492	91,571.53	873.3859	981.2158	7.049893
f14	Best	0.492069	5682.04	571.0485	1.759394	115.4002	0.016531
	Mean	2.975573	4367.468	637.6884	30.75647	118.1058	0.071366
f15	Best	0.180927	6164.711	6200.941	2457.498	2580.792	1.557302
	Mean	1.096115	3.15E + 08	67,382.34	2491.902	6,305,865	0.934786
f16	Best	86.55439	3706.789	3833.025	1231.729	1305.865	2.65E-07
	Mean	86.6231	2.04E + 08	6.1E + 10	1331.846	4,080,172	0.00321
f17	Best	0.09995	2463.619	2565.265	4108.524	4157.796	4.05E-10
	Mean	0.755612	2959.807	32,021.85	4115.572	4174.768	0.003185
f18	Best	0.285803	4935.755	5737.945	1645.049	1743.764	1.576064
	Mean	0.230461	8.37E + 08	58,653.45	1689.196	16,744,092	7.73E-07
f19	Best	84.58424	2472.14	2587.482	960.9384	1010.381	1.297055
	Mean	84.587	1.07E + 09	28,226.82	879.5446	21,367,903	1.055225
f20	Best	294.098	2.37E-05	1.55E-05	1.19E-05	1.23E-05	1.88E-06
	Mean	294.139	2.9E-05	1.91E-05	0.352457	0.352457	1.35E-06
f21	Best	417.2918	2512.619	2538.59	872.9317	923.1841	2.20E-13
	Mean	417.2919	3348.184	44,399.19	874.096	941.0597	1.166838
f22	Best	717.3037	3051.619	3187.129	1412.285	1473.317	0.021739
	Mean	717.3881	3694.798	34,993.43	1413.852	1487.748	0.007397
f23	Best	980.6591	2.76E-05	0.000233	15.42417	15.42417	1.39E-06
	Mean	981.4909	0.000559	0.000586	18.3773	18.37731	5.31E-06
f24	Best	1068.116	4.41E-06	2.24E-05	384.4512	384.4512	1.88E-07
	Mean	1068.439	8.21E-06	2.83E-05	892.0024	892.0024	1.98E-07

Table 4 (continued)

Function	Fitness	DE	WOA	LION	PSO	ACSA	LXLOA
f25	Best	0.003788	1.03E-05	1.64E-06	0.424411	0.424411	1.48E-07
	Mean	0.005067	9.29E-05	1.77E-06	0.002573	0.002574	2.5E-07
f26	Best	1471.335	3.25E-05	8.13E-06	14.21998	14.21998	1.81E-08
	Mean	1471.942	1.13E-05	8.91E-06	129.9557	129.9557	1.89E-08
f27	Best	294.1373	3.45E-08	1.08E-07	5.64E-11	7.46E-10	2.21E-15
	Mean	295.2326	4.13E-08	4.44E-07	1.99E-11	8.45E-10	1.89E-14
f28	Best	2.81E-08	2.17E + 08	2.33E-06	3.38E-08	4,344,904	4.78E-12
	Mean	2.94E-08	8.59E-08	1.45E-07	3.38E-08	3.56E-08	3.68E-12
f29	Best	1912.455	6.3E + 08	3.18E + 10	4.69E + 10	4.69E + 10	480.505
	Mean	1853.655	4.7E + 10	3.22E + 10	5,647,528	9.46E + 08	395.05

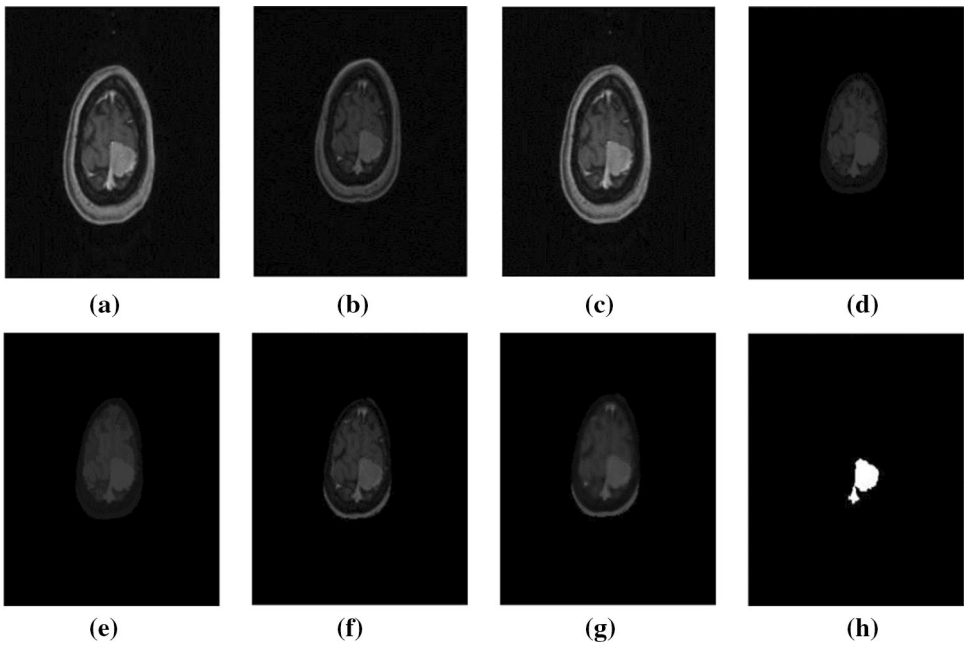

Fig. 3 Tumored brain MRI sample Images. **a** Normalization of brain MRI image; **b** Extended Weiner filtering; **c** Segmented image using LXLOA **d**–**e** Mathematical morphological operations; **f** Extracted skull stripped image; **g** Anisotropic diffusion; and **h** Feature extraction

significantly better results than PSO, ACSA, WOA, and LION algorithms. In addition, we can see the performance of algorithm's pair LXLOA-DE is not significantly better but the proposed LXLOA showed good results over DE. The performance significance is represented by yellow line in Fig. 5 connecting pair of algorithms.

Pairwise tests have been conducted and results have been reported in Tables 11, 12, 13, 14 respectively for Wilcoxon test on fitness values and Kruskal–Wallis test on mean and best fitness values. Five pairs have been created: LXLOA—ACSA, LXLOA—DE, LXLOA—LOA, LXLOA—PSO, and LXLOA—WOA. It can be seen that the p-value of each pair is less than 0.05. It indicates that the performance of the proposed LXLOA is statistically significant at a 95% level of significance. It can be noted that the proposed LXLOA showed better performance by achieving higher value of standard deviation as compared to other algorithms. Therefore, based on this observation, LXLOA is more stable and robust.

4.4 Quality metrics

Three quality metrics: (a) fitness values; (b) PSNR value; and (c) SSIM values were chosen for evaluating the performance. Fitness values to assess the optimal threshold value of the image quantitatively. The evaluation function

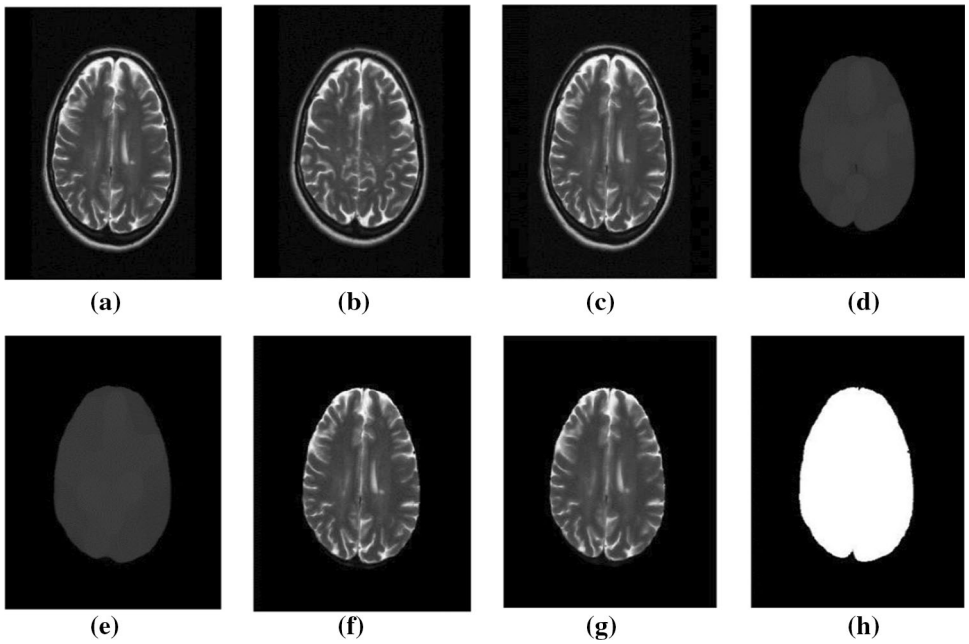

Fig. 4 Non-tumored Brain MRI sample Images. **a** Normalization of brain MRI image; **b** Extended weiner filtering; **c** Segmented image using LXLOA **d**–**e** Mathematical morphological operations; **f** Extracted skull stripped image **g** Anisotropic diffusion; and **h** Feature extraction

Table 5 Features extracted sample IBSR data the IBSR and MS free sample images using GLCM Method

Sl. No Image	Cluster prominence	Auto correlation	Correlation	Contrast	Cluster Shade	Homogeneity
1	1.2454	1.4426	0.015595	0.9913	0.00218	− 0.9646
2	1.3198	1.6215	0.02815	0.9867	0.00437	− 0.9467
3	1.2777	1.514	0.04639	0.9722	0.00795	− 0.9041
4	1.2896	1.5231	0.035416	0.9801	0.00575	− 0.9271
5	1.2889	1.5027	0.018384	0.9905	0.00265	− 0.9611
6	1.3228	1.6481	0.023017	0.9898	0.00345	− 0.9572
7	1.31	1.6836	0.040468	0.9809	0.00675	− 0.927
8	1.2992	1.7636	0.021899	0.9914	0.00325	− 0.9622
9	1.3094	1.7211	0.027616	0.9883	0.00428	− 0.9512
10	1.3078	1.7348	0.023256	0.9906	0.00349	− 0.9592
11	1.3111	1.7232	0.023097	0.9905	0.00346	− 0.9592
12	1.3208	1.6873	0.0188	0.9923	0.00272	− 0.966
13	1.3164	1.7116	0.018051	0.9928	0.00259	− 0.9679
14	1.3162	1.6907	0.026926	0.9883	0.00415	− 0.9515
15	1.3194	1.6633	0.027692	0.9876	0.00429	− 0.9492
16	1.3137	1.6867	0.032938	0.9851	0.00527	− 0.9406
17	1.3143	1.7101	0.023017	0.9905	0.00345	− 0.959
18	1.3123	1.6304	0.041724	0.979	0.00700	− 0.9219
19	1.162	1.3847	0.043454	0.9674	0.00735	− 0.8949
20	1.3148	1.633	0.037642	0.9815	0.00618	− 0.9296

Table 6 Feature extraction of sample IBSR data the IBSR and MS free sample images using GLCM Method

Entropy	Energy	Dissimilarity	Sum entropy	Sum average	Maximum pobability
0.9989	0.4339	0.74576	0.126	0.4324	2.2958
0.9978	0.5384	0.66628	0.1647	0.5354	2.4158
0.996	0.5042	0.7064	0.1429	0.4987	2.3453
0.9971	0.4981	0.70511	0.1446	0.4941	2.3507
0.9987	0.4703	0.71781	0.1398	0.4685	2.336
0.9983	0.545	0.65717	0.1697	0.5426	2.4332
0.9966	0.5774	0.64018	0.1766	0.5727	2.458
0.9984	0.5893	0.61674	0.19	0.587	2.5101
0.9979	0.5793	0.62982	0.183	0.5763	2.4822
0.9983	0.5801	0.62603	0.1852	0.5777	2.4911
0.9983	0.5755	0.63005	0.1833	0.5731	2.4833
0.9986	0.5571	0.64356	0.1769	0.5552	2.4591
0.9987	0.566	0.63508	0.1812	0.5642	2.4753
0.9979	0.5666	0.64067	0.1776	0.5637	2.4618
0.9979	0.5561	0.65051	0.1726	0.5531	2.4436
0.9974	0.571	0.64079	0.177	0.5674	2.4596
0.9983	0.5704	0.63459	0.181	0.568	2.4746
0.9965	0.556	0.65975	0.1667	0.5511	2.4226
0.9963	0.4259	0.76729	0.1127	0.4208	2.2589
0.9969	0.553	0.65968	0.1671	0.5488	2.4241

Table 7 Feature extraction of sample IBSR data and MS free sample images using GLCM Method

Sum of Square Variance	Inverse difference	Imc 2	Imc 1	Difference variance	Difference entropy
0.50192	0.851	0.9989	0.7446	0.002189	0.0021846
0.65435	0.7899	0.9978	0.7875	0.004379	0.0043596
0.56345	0.82335	0.996	0.7515	0.007958	0.0078942
0.57259	0.8218	0.9971	0.7597	0.005754	0.005721
0.55643	0.83068	0.9987	0.7623	0.002653	0.0026455
0.67534	0.78165	0.9983	0.7952	0.003453	0.0034406
0.69949	0.76762	0.9966	0.7945	0.006751	0.006705
0.75677	0.74331	0.9984	0.8153	0.003256	0.0032454
0.72756	0.75678	0.9979	0.8064	0.004281	0.0042622
0.73748	0.75273	0.9983	0.8104	0.003495	0.0034824
0.72953	0.75663	0.9983	0.8086	0.003467	0.0034545
0.70473	0.76908	0.9986	0.8043	0.002723	0.0027153
0.72207	0.76106	0.9987	0.8087	0.002596	0.0025896
0.70622	0.76701	0.9979	0.8015	0.004154	0.004137
0.68613	0.77605	0.9979	0.7961	0.004295	0.0042761
0.70265	0.76758	0.9974	0.7983	0.005277	0.0052491
0.72048	0.76099	0.9983	0.8065	0.003453	0.0034406
0.6596	0.7852	0.9965	0.7833	0.007003	0.0069542
0.44347	0.86685	0.9963	0.7059	0.007354	0.0073
0.66214	0.78486	0.9969	0.7857	0.006189	0.0061509

Table 8 Feature extraction of sample IBSR data the IBSR and MS free sample images using GLDM Method

S.N Image	Grid-weighted sum	Diagonal-weighted sum	Vertical-weighted sum	Horizontal-weighted sum	Cluster prominence
1	142,000	143,000	142,000	142,000	0.70536
2	142,000	142,000	142,000	142,000	0.76196
3	141,000	142,000	141,000	142,000	0.73254
4	142,000	142,000	142,000	142,000	0.73989
5	142,000	143,000	142,000	142,000	0.7372
6	142,000	142,000	142,000	142,000	0.76354
7	141,000	142,000	141,000	142,000	0.75458
8	142,000	142,000	142,000	142,000	0.73985
9	142,000	142,000	142,000	142,000	0.75131
10	142,000	142,000	142,000	142,000	0.7489
11	142,000	142,000	142,000	142,000	0.75214
12	142,000	143,000	142,000	142,000	0.76087
13	142,000	143,000	142,000	142,000	0.75641
14	142,000	142,000	142,000	142,000	0.7579
15	142,000	142,000	142,000	142,000	0.76113
16	142,000	142,000	142,000	142,000	0.75663
17	142,000	142,000	142,000	142,000	0.7553
18	142,000	142,000	141,000	142,000	0.75767
19	141,000	142,000	141,000	142,000	0.65183
20	142,000	142,000	142,000	142,000	0.7591

is used for determining the optimal fitness score of the image. PSNR [71] quantifies the standard of reconstructed segmented image quality using the minimized value of root mean squared error as shown in Eqs. (14) and (15), respectively. A higher value of PSNR indicates that an improved reconstructed image is obtained with better quality.

$$\text{PSNR} = 20\left(\frac{255}{\text{RMSE}}\right) \tag{14}$$

$$\text{RMSE} = \sqrt{\sum_{x=1}^{p}\sum_{y=1}^{Q}\frac{(B(x,y)-B'(x,y))^2}{P.Q}} \tag{15}$$

B is the original image, and B' is the segmented image with a size P*Q.

SSIM [72] determines the similarity between two reconstructed and original images. The mathematical formulation is represented in Eq. (16). A higher value of SSIM determines the more structural similarity and edge information of the segmented image.

$$\text{SSIM}(B,B') = (2\mu_B + n_1) + 2(2\sigma_B\sigma_{B'} + n_2)/(\mu_B^2 + \mu_{B'}^2 + n_1)(\sigma_B^2 + \sigma_{B'}^2 + n_2) \tag{16}$$

Here, $\mu_B(\mu_{B'})$ shows the mean intensity and $\sigma_B(\sigma_{B'})$ represents the standard deviation of brain MRI image B (B'). The constants values of n_1 and n_2 taken are 6.5025 and 58.5225.

4.5 Comparative results and analysis

The comparative result computation of different metrics measures is reported in this section. Table 15 shows the average fitness value of the segmented image. Table 16 shows the average PSNR values for measuring the image quality. Table 17 presents the comparative analysis of average SSIM values estimating the structural similarity depending on the reconstructed image intensities. Each sample image shows the average value of 20 images. The observation states that LXLOA provides higher PSNR and SSIM values which gives better image quality. Table 18 computation provides the Jaccard coefficient and dice similarity values for validation purpose. The quantitative

Table 9 Optimized feature subset showing min, max and average value of the IBSR and MS free sample images

Sl. No Image	Auto correlation			Sum average			Vertical weighted			Diagonal weighted			Grid weighted		
	Min	Max	Avg	Min	Max	Avg	Min	Max	Avg	Min	Max	Avg	Min	Max	Avg
1	1.4426	1.622	1.5208	2.2958	2.416	2.3487	141,370	142,310	141,910	141,750	142,570	142,230	141,210	142,280	141,886
2	1.6481	1.764	1.7102	2.4332	2.51	2.4749	141,370	142,180	141,950	141,920	142,420	142,278	141,480	142,160	141,954
3	1.6633	1.723	1.6952	2.4436	2.483	2.4646	141,910	142,280	142,102	142,270	142,510	142,392	141,860	142,270	142,080
4	1.3847	1.71	1.609	2.2589	2.475	2.408	141,960	142,080	141,586	141,840	142,390	142,050	141,290	142,140	141,676
5	1.1554	2.119	1.7503	2.1046	2.747	2.5017	141,160	261,090	260,322	259,840	261,500	260,936	258,830	261,160	260,382
6	1.6398	1.941	1.7953	2.4273	2.628	2.531	258,880	261,220	261,108	261,420	264,550	261,478	261,110	261,250	261,170
7	1.5066	1.976	1.749	2.3386	2.652	2.5007	260,990	261,120	260,466	260,490	261,470	261,070	259,730	261,110	260,480
8	1.6226	1.961	1.8014	2.4179	2.641	2.5355	259,740	261,160	260,630	259,940	261,570	261,188	259,040	261,160	260,694
9	1.2519	2.141	1.5389	2.1687	2.762	2.3608	258,870	261,000	142,750	65,336	261,420	143,283	65,186	261,050	142,803
10	1.1993	4	1.7759	2.1335	4	2.5178	65,212	65,536	65,350	65,388	65,536	65,426	65,266	65,536	65,330.4
11	4	4	4	4	4	4	65,288	65,536	65,536	65,536	65,536	65,536	65,536	65,536	65,536
12	4	4	4	4	4	4	65,536	65,536	65,536	65,536	65,536	65,536	65,536	65,536	65,536
13	1.2831	4	2.3834	2.1897	4	2.9229	65,102	65,536	65,323.2	65,256	65,536	65,402.8	65,084	65,536	65,299.6
14	1.2322	4	2.8978	2.1556	4	3.2655	65,254	65,536	65,429.2	65,370	65,536	65,472.4	65,242	65,536	65,423.6
15	1.3212	1.38	1.353	2.2151	2.254	2.2363	65,190	65,246	65,216.8	65,316	65,370	65,343.2	65,176	65,224	65,197.2
16	1.2398	1.311	1.2756	2.1605	2.208	2.1845	65,262	65,296	65,276	65,378	65,402	65,388	65,244	65,276	65,258.8
17	1.2215	4	3.4443	2.1483	4	3.6297	65,302	65,536	65,489.2	65,406	65,536	65,510	65,284	65,536	65,485.6
18	1.3524	4	2.9434	2.2358	4	3.296	65,208	65,536	65,408	65,346	65,536	65,463.6	65,220	65,536	65,412
19	1.2809	1.34	1.3096	2.188	2.228	2.2072	65,158	65,260	65,228.2	65,300	65,388	65,360.4	65,194	65,270	65,242.8
20	1.2127	4	1.7904	2.1425	4	2.5275	65,258	65,536	65,319.6	65,386	65,536	65,419.6	65,268	65,536	65,331.6

Table 10 Independent samples Kruskal–Wallis test

S.N	Null hypothesis	Test	Sig	Decision
1	The distribution of Best_Fitness is the same across categories of algorithms	Independent-samples Kruskal–Wallis test	0.000	Reject the null hypothesis

Asymptotic significances are displayed. The significance level is 0.05

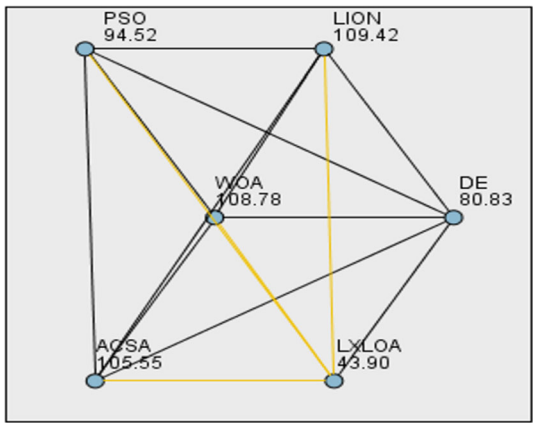

Fig. 5 Pairwise comparison of algorithms

Table 11 Wilcoxon test on best fitness values

Algorithm (A)	Algorithm (B)	SD	*p*-value
LXLOA	ASCA	16	0
	DE	64	0
	LOA	5	0
	PSO	21	0
	WOA	15	0

SD standard deviation

Table 12 Wilcoxon test on mean fitness values

Algorithm (A)	Algorithm (B)	SD	*p*-value
LXLOA	ASCA	7	0
	DE	58	0
	LOA	1	0
	PSO	18	0
	WOA	21	0

SD standard deviation

Table 13 Kruskal–Wallis test on best fitness values

Algorithm (A)	Algorithm (B)	SD	*p*-value
LXLOA	ASCA	23	0
	DE	11	0
	LOA	17	0
	PSO	16	0
	WOA	18	0

SD standard deviation

Table 14 Kruskal-Wall Test on mean fitness values

Algorithm (A)	Algorithm (B)	SD	*p*-value
LXLOA	ASCA	21	0
	DE	9	0
	LOA	13	0
	PSO	15	0
	WOA	13	0

SD standard deviation

assessment performance metrics consider the similarity of the reconstructed outcome image with a corresponding ground image.

Table 19 depicts the comparative analysis of classification methods (SVM and ANN) on the proposed technique's selected features (Algorithm 2). Results reveal that the ANN outperforms the SVM. ANN gives (a) accuracy (97.37%), (b) sensitivity (85.8%), (c) specificity (90%) and (d) precision (91.92%).

The computational time of the algorithms is presented in Table 20. It can be seen that time taken by the proposed LXLOA (181.4101) is lesser than the other meta-heuristic algorithms. This result indicates that the LXLOA has a higher tendency of convergence to the global optimum. We noted that the convergence speed of the DE is worst because it took maximum computational time to reach the global solution. So it can be concluded that the proposed

Table 15 Comparative analysis of average fitness values on brain MRI sample images using different metaheuristics techniques

Sample image	DE	WOA	PSO	LOA	ACSA	LXLOA
Image 1	3.31	1.936	3.6975	4.2783	4.285695	4.332092
Image 2	1.127	3.6716	4.6968	5.79828	5.807674	5.047576
Image 3	5.093	6.242	5.7309	7.6035	7.614962	8.376435
Image 4	1.0882	4.2876	4.6976	5.98388	5.993275	8.425117
Image 5	1.2737	4.2864	4.7112	5.99712	6.006542	13.52087
Image 6	0.34316	4.287	4.7103	5.9964	6.005821	5.857293
Image 7	0.20226	4.288	4.7055	5.9919	6.001311	8.299372
Image 8	1.0333	4.3026	4.6991	5.98988	5.999278	9.316846
Image 9	0.39789	4.2911	4.7175	6.00483	6.014265	8.572981
Image 10	0.34316	4.287	4.7103	5.9964	6.005821	5.857293
Image 11	0.20226	4.288	4.7055	5.9919	6.001311	8.299372
Image 12	0.33545	4.2871	4.6995	5.98563	5.995029	7.578636
Image 13	2.2837	4.9864	4.6151	6.11102	6.12025	6.286947
Image 14	1.36116	4.2987	4.6103	5.89991	5.909131	5.958293
Image 15	1.20226	4.2955	4.9455	6.23415	6.244041	7.794372
Image 16	1.4333	4.8926	4.3191	5.78688	5.795518	8.751246
Image 17	0.46189	4.2911	4.875	6.16233	6.17208	8.724481
Image 18	0.50116	4.897	4.6103	6.0794	6.088621	5.857293
Image 19	0.69746	4.848	4.8475	6.3019	6.311595	7.289372
Image 20	0.71746	3.884	3.9465	5.1117	5.119593	5.273513

Table 16 Comparative analysis with respect to average PSNR values on brain MRI sample images

Sample image	DE	WOA	PSO	LOA	ACSA	LXLOA
Image 1	15.265	20.6	18.998	19.0186	19.0566	20.89488
Image 2	15.47	20.89	20.82	20.84089	20.88253	23.06032
Image 3	15.66	21.275	21.2	21.22128	21.26368	23.2098
Image 4	15.843	20.912	21	21.02091	21.06291	23.13809
Image 5	16.075	20.788	20.788	20.80879	20.85036	20.99588
Image 6	16.466	21.109	21.109	21.13011	21.17233	21.32009
Image 7	16.964	20.599	20.599	20.6196	20.6608	20.80499
Image 8	17.539	18.23	18.306	18.32423	18.36084	21.57966
Image 9	23.15	24.546	23.51	23.53455	23.58157	29.84146
Image 10	22.809	22.909	23.009	23.03191	23.07793	24.22788
Image 11	21.8	22.898	22.762	22.7849	22.83042	25.14698
Image 12	22.3	22.2	20.244	20.2662	20.30669	25.49644
Image 13	17.075	20.888	20.988	21.00889	21.05086	21.90488
Image 14	16.886	20.235	20.219	20.23924	20.27967	21.41099
Image 15	15.964	21.689	21.698	21.71969	21.76309	22.81489
Image 16	17.639	18.353	18.386	18.40435	18.44113	19.50916
Image 17	25.15	26.546	26.51	26.53655	26.58957	30.18789
Image 18	22.829	22.929	23.315	23.33793	23.38456	24.15718
Image 19	21.9	22.998	22.962	22.985	23.03092	24.94498
Image 20	15.466	20.119	20.823	20.84312	20.88477	21.58269

Table 17 Comparative analysis with respect to average SSIM values on brain MRI sample images

Sample image	DE	WOA	PSO	LOA	ACSA	LXLOA
Image 1	0.33822	0.44141	0.44111	0.441551	0.442434	0.448612
Image 2	0.33717	0.44757	0.44735	0.447798	0.448692	0.453844
Image 3	0.33173	0.44943	0.4484	0.448849	0.449746	0.455348
Image 4	0.33054	0.45715	0.45261	0.453067	0.453972	0.463196
Image 5	0.32771	0.46507	0.46619	0.466655	0.467587	0.472569
Image 6	0.43511	0.47034	0.47665	0.47712	0.478074	0.490911
Image 7	0.357	0.47654	0.46709	0.467567	0.468501	0.572791
Image 8	0.4772	0.48483	0.50017	0.500655	0.501655	0.707172
Image 9	0.40819	0.48708	0.41066	0.411147	0.411968	0.726079
Image 10	0.41558	0.48748	0.41926	0.419748	0.420586	0.726412
Image 11	0.41733	0.69748	0.42101	0.421708	0.42255	0.73422
Image 12	0.41292	0.69412	0.63496	0.635654	0.636924	0.739482
Image 13	0.4152	0.49708	0.4906	0.491097	0.492078	0.75345
Image 14	0.4156	0.48758	0.41896	0.419448	0.420286	0.664782
Image 15	0.45143	0.74856	0.5101	0.510849	0.511869	0.777044
Image 16	0.5192	0.65693	0.6996	0.700257	0.701656	0.840482
Image 17	0.45819	0.46708	0.46066	0.461127	0.462048	0.736179
Image 18	0.4658	0.4748	0.4926	0.493075	0.49406	0.719322
Image 19	0.4156	0.6986	0.421	0.421699	0.422541	0.73326
Image 20	0.43717	0.46557	0.46535	0.465816	0.466746	0.473034

Table 18 Shows the average Jaccard Coefficient and Dice similarity values for IBSR and MS free data images

Sample image	Dice coefficient	Jaccard coefficient
Image 1	0.99339	0.98686
Image 2	0.99182	0.98378
Image 3	0.99236	0.98483
Image 4	0.99233	0.98477
Image 5	0.99251	0.98512
Image 6	0.99271	0.98553
Image 7	0.9937	0.98749
Image 8	0.99154	0.98323
Image 9	0.99191	0.98395
Image 10	0.99206	0.98424
Image 11	0.99235	0.98482
Image 12	0.99092	0.98199
Image 13	0.9985	0.98414
Image 14	0.99568	0.982
Image 15	0.9964	0.99
Image 16	0.9959	0.98986
Image 17	0.99282	0.98578
Image 18	0.992436	0.984583
Image 19	0.99235	0.98677
Image 20	0.99451	0.98612

Table 19 Classification of result with respect to selected features for determining tumored and non-tumored MRI

Parameters	SVM	ANN
Sensitivity	79.2	85.8
Specificity	86.625	90
Precision	91.38461	91.92857
Accuracy	92.0898	97.3269

LXLOA is a cost-effective computational method, and it can converge to a global optimum solution quickly.

4.6 Discussion and analysis

Figure 2 presents the proposed methodology flow process to detect and predict brain tumor using MRI images. The consolidated steps of the proposed method are shown in Algorithm 1. The simulated analysis at each successive stage for the skull stripping technique on IBSR and MS free dataset is shown in Figs. 3 and 4, respectively. The extracted texture and statistical feature are depicted in Tables 5, 6, 7, 8 respectively, and optimized features

Table 20 Comparison of efficiency with respect to time taken by different meta-heuristic technique

Algorithm	DE	WOA	PSO	LOA	ACSA	LXLOA
Average time taken in seconds	200.646	186.3541	195.6152	188.568	185.648	181.4101

selected through Fuzzy weighted k-means embedding LDA (Algorithm 2) are shown in Table 9. The visualization analysis of average fitness function, PSNR, and SSIM are depicted in Fig. 6a, b, c for comparative analysis of existing metaheuristics such as DE, WOA, PSO, LOA, ACSA, and LXLOA. The observation shows the proposed algorithm is providing promising results compared to other methods. The validation of the proposed algorithm is attained by evaluating the similarity between the ground truth image and segmented image, as depicted in Fig. 7. Moreover, Fig. 8 presents that the artificial neural network gives better performance measures on a comparative study with support vector machine.

5 Conclusions

In this paper, an approach for the intelligent computer-aided mechanism has been developed to diagnose and detect tumor and non-tumored brain MRI images to take preventive measures at an early stage. Extended Weiner filtering technique is proposed for improving the quality of image dataset needed to be analyzed. Further, LXLOA was proposed to improve efficiency and provide the optimal threshold value for segmentation of the tumor region. The optimized set of features were extracted from segmented using effective fuzzy weighted k-means embedding LDA algorithm and, it helped in the decision-making process. Extensive simulations were conducted to determine the effectiveness of the proposed algorithm. To present a fair outcome, results were validated using different parameters. LXLOA is tested on 29 standard functions and compared with different metaheuristics algorithms such as DE, WOA, PSO, LOA, ACSA, and LXLOA. The performance was measured using three quality metrics (a) fitness, (b) PSNR, (c) SSIM and validated using different coefficient parameters. The observation determines that LXLOA outperforms the existing state of the art and generates better computational efficiency. The best feature subset was selected using fuzzy k-means embedding LDA algorithm giving improved classification computation. Results revealed that LXLOA showed promising results by attaining accuracy of 97%. Thus, the proposed algorithm is providing promising experimental analysis and outcomes. The immediate future extension involves the usage of 3-dimensional (3-D) medical data for clinical research by incorporating the improved metaheuristics algorithms.

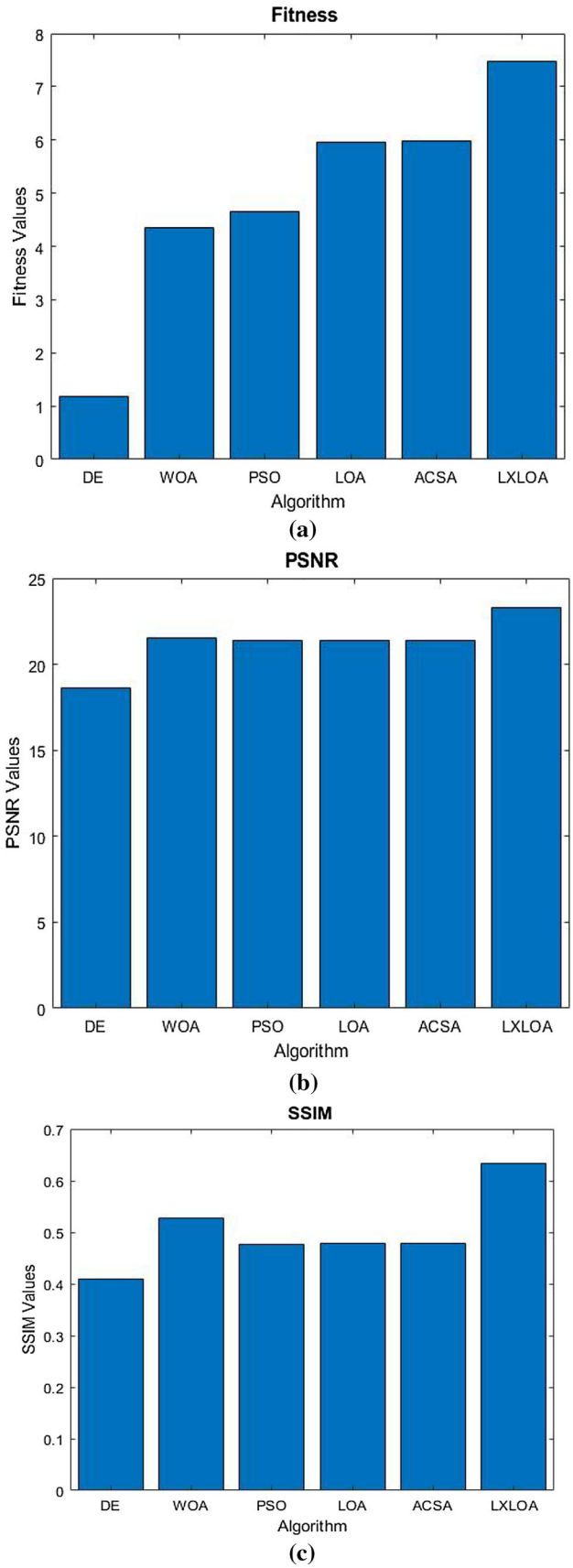

◀**Fig. 6** Representation of average results obtained on comparative analysis using different metaheuristics technique. **a** average fitness value; **b** average PSNR; and **c** average SSIM

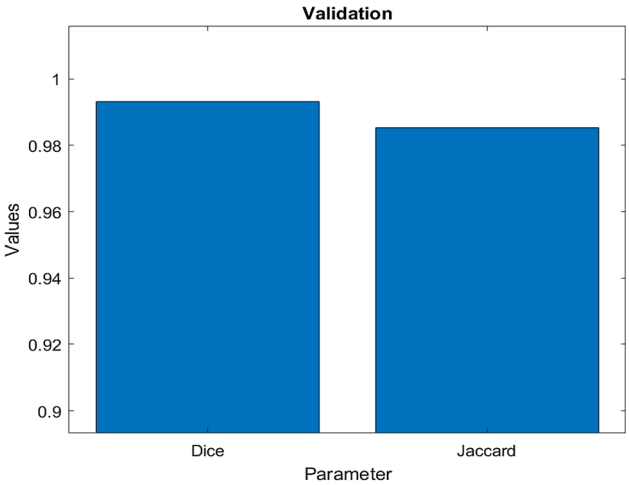

Fig. 7 Validation using dice coefficient and jaccard coefficient

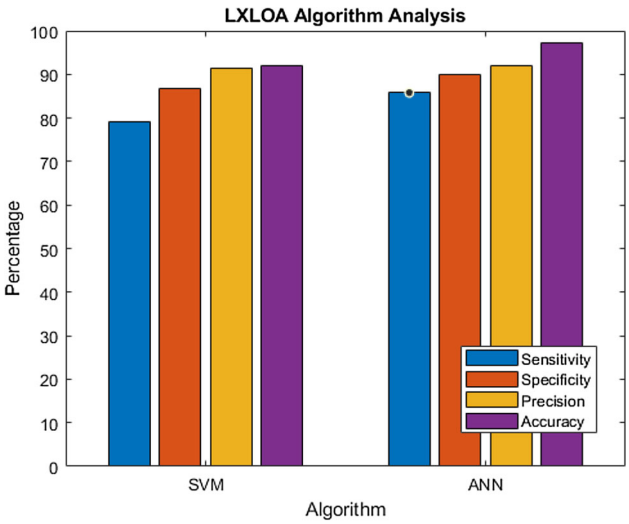

Fig. 8 Performance measures with reference to algorithm

Declarations

Conflict of interest The authors declare that they have no conflict of interest.

References

1. Erickson BJ, Korfiatis P, Akkus Z, Kline TL (2017) Machine learning for medical imaging. Radiographics 37(2):505–515
2. Giger ML (2018) Machine learning in medical imaging. J Am Coll Radiol 15(3):512–520

3. Kumar A, Bi L, Kim J, Feng DD (2020) Machine learning in medical imaging. In: Feng DD (ed) Biomedical information technology. Academic Press, Cambridge, pp 167–196
4. McAuliffe MJ, Lalonde FM, McGarry D, Gandler W, Csaky K, Trus BL (2001) Medical image processing, analysis and visualization in clinical research. In: Proceedings 14th IEEE symposium on computer-based medical systems. CBMS 2001 (pp. 381–386). IEEE
5. Bhattacharyya S, Konar D, Platos J, Kar C, Sharma K (eds) (2020) Hybrid machine intelligence for medical image analysis. Springer, Berlin
6. Schmidhuber J (2015) Deep learning in neural networks: an overview. Neural Netw 61:85–117
7. Bagchi S, Tay KG, Huong A, Debnath SK (2020) Image processing and machine learning techniques used in computer-aided detection system for mammogram screening-A review. Int J Electr Comput Eng 10(3):2336
8. Hatt M, Parmar C, Qi J, El Naqa I (2019) Machine (deep) learning methods for image processing and radiomics. IEEE Trans Radiat Plasma Med Sci 3(2):104–108
9. Latif J, Xiao C, Imran A, Tu S (2019) Medical imaging using machine learning and deep learning algorithms: a review. In: 2019 2nd International conference on computing, mathematics and engineering technologies (iCoMET) (pp. 1–5). IEEE
10. Lundervold SA, Lundervold A (2018) An overview of deep learning in medical imaging focusing on MRI. arXiv, arXiv:1811
11. Roy S, Bandyopadhyay SK (2012) Detection and quantification of brain tumor from MRI of brain and it's symmetric analysis. Int J Info Commun Technol Res 2(6)
12. Despotović I, Goossens B, Philips W (2015) MRI segmentation of the human brain: challenges, methods, and applications. Comput Math Methods Med 2015:1–23
13. Patel J, Doshi K (2014) A study of segmentation methods for detection of tumor in brain MRI. Adv Electron Electr Eng 4(3):279–284
14. Lei B, Fan J (2019) Image thresholding segmentation method based on minimum square rough entropy. Appl Soft Comput 84:105687
15. Park JG, Lee C (2009) Skull stripping based on region growing for magnetic resonance brain images. Neuroimage 47(4):1394–1407
16. Ahmmed R, Swakshar AS, Hossain MF, Rafiq MA (2017) Classification of tumors and it stages in brain MRI using support vector machine and artificial neural network. In: 2017 International conference on electrical, computer and communication engineering (ECCE) (pp. 229–234). IEEE
17. Qin AK, Huang VL, Suganthan PN (2008) Differential evolution algorithm with strategy adaptation for global numerical optimization. IEEE Trans Evol Comput 13(2):398–417
18. Sharawi M, Zawbaa HM, Emary E (2017) Feature selection approach based on whale optimization algorithm. In: 2017 Ninth international conference on advanced computational intelligence (ICACI) (pp. 163–168). IEEE
19. Trelea IC (2003) The particle swarm optimization algorithm: convergence analysis and parameter selection. Inf Process Lett 85(6):317–325
20. Boothalingam R (2018) Optimization using lion algorithm: a biological inspiration from lion's social behavior. Evol Intel 11(1–2):31–52
21. Hu G, Wu J, Li H, Hu X (2020) Shape optimization of generalized developable H- Bézier surfaces using adaptive cuckoo search algorithm. Adv Eng 149:102889
22. El Aziz MA, Ewees AA, Hassanien AE (2018) Multi-objective whale optimization algorithm for content-based image retrieval. Multimed Tools Appl 77(19):26135–26172
23. Fister Jr I, Yang XS., Fister I, Brest J, Fister D (2013) A brief review of nature- inspired algorithms for optimization. arXiv preprint arXiv:1307.4186.
24. Ramson SJ, Raju KL, Vishnu S, Anagnostopoulos T (2019) Nature inspired optimization techniques for image processing—A short review. In: Hemanth J, Balas VE (eds) Nature inspired optimization techniques for image processing applications. Springer, Cham, pp 113–145
25. Nayyar A, Puri V, Suseendran G (2019) Artificial bee colony optimization— population-based meta-heuristic swarm intelligence technique. In: Balas VE, Sharma N, Chakrabarti A (eds) Data management, analytics and innovation. Springer, Singapore, pp 513–525
26. Karaboga D, Gorkemli B, Ozturk C, Karaboga N (2014) A comprehensive survey: artificial bee colony (ABC) algorithm and applications. Artif Intell Rev 42(1):21–57
27. Karaboga D, Basturk B (2007) Artificial bee colony (ABC) optimization algorithm for solving constrained optimization problems. In: Melin P, Castillo O, Aguilar LT, Kacprzyk J, Pedrycz W (eds) International fuzzy systems association world congress. Springer, Berlin, pp 789–798
28. Karaboga D, Basturk B (2008) On the performance of artificial bee colony (ABC) algorithm. Appl Soft Comput 8(1):687–697
29. Junior FEF, Yen GG (2019) Particle swarm optimization of deep neural networks architectures for image classification. Swarm Evol Comput 49:62–74
30. Mirjalili S, Lewis A (2016) The whale optimization algorithm. Adv Eng Softw 95:51–67
31. Lai CC, Tseng DC (2004) A hybrid approach using Gaussian smoothing and genetic algorithm for multi-level thresholding. Int J Hybrid Intell Syst 1(3–4):143–152
32. Zhan ZH, Zhang J, Li Y, Chung HSH (2009) Adaptive particle swarm optimization. IEEE Trans Syst, Man, Cybern, Part B (Cybernetics) 39(6):1362–1381
33. Dhal KG, Das A, Ray S, Das S (2019) A clustering based classification approach based on modified cuckoo search algorithm. Pattern Recognit Image Anal 29(3):344–359
34. Kavuturu KK, Narasimham PVRL (2020) Multi-objective economic operation of modern power system considering weather variability using adaptive cuckoo search algorithm. J Electr Syst Inf Technol 7(1):1–29
35. Al-Tashi Q, Rais HM, Abdulkadir SJ, Mirjalili S, Alhussian H (2020) A review of grey wolf optimizer-based feature selection methods for classification. In: Mirjalili S, Faris H, Aljarah I (eds) Evolutionary machine learning techniques. Springer, Singapore, pp 273–286
36. Ahmed AM, Rashid TA, Saeed SAM (2020) Cat swarm optimization algorithm: a survey and performance evaluation. Comput Intell Neurosci 2020:1–20
37. Yazdani M, Jolai F (2016) Lion optimization algorithm (LOA): a nature-inspired metaheuristic algorithm. J Comput Des Eng 3(1):24–36
38. Vijh S, Gaurav P, Pandey HM (2020) Hybrid bio-inspired algorithm and convolutional neural network for automatic lung tumor detection. Neural Comput Appl. https://doi.org/10.1007/s00521-020-05362-z
39. Pandey HM, Chaudhary A, Mehrotra D (2014) A comparative review of approaches to prevent premature convergence in GA. Appl Soft Comput 24:1047–1077
40. Wang G, Li W, Ourselin S, Vercauteren T (2017) Automatic brain tumor segmentation using cascaded anisotropic convolutional neural networks. In: International MICCAI brainlesion workshop (pp. 178–190). Springer, Cham
41. Kumar V, Sachdeva J, Gupta I, Khandelwal N, Ahuja CK. (2011). Classification of brain tumors using PCA-ANN. In: 2011

World congress on information and communication technologies (pp. 1079–1083). IEEE
42. Sharma A, Kumar S, Singh SN (2018) Brain tumor segmentation using DE embedded OTSU method and neural network. Multidimens Syst Signal Process 30:1263–1291
43. El Abbadi NK, Kadhim NE (2017) Brain cancer classification based on features and artificial neural network. Brain 6(1):123–134
44. Lashkari A (2010) A neural network based method for brain abnormality detection in MR images using Gabor wavelets. Int J Comput Appl 4(7):9–15
45. Vijh S, Sharma S, Gaurav P (2020) Brain tumor segmentation using OTSU embedded adaptive particle swarm optimization method and convolutional neural network. In: Hemanth J, Bhatia M, Geman O (eds) Data visualization and knowledge engineering. Springer, Cham, pp 171–194
46. Zhao X, Wu Y, Song G, Li Z, Zhang Y, Fan Y (2018) A deep learning model integrating FCNNs and CRFs for brain tumor segmentation. Med Image Anal 43:98–111
47. Loizou CP, Petroudi S, Seimenis I, Pantziaris M, Pattichis CS (2015) Quantitative texture analysis of brain white matter lesions derived from T2-weighted MR images in MS patients with clinically isolated syndrome. J Neuroradiol 42(2):99–114
48. Manic KS, Priya RK, Rajinikanth V (2016) Image multithresholding based on Kapur/Tsallis entropy and firefly algorithm. Indian J Sci Technol 9(12):89949
49. Soleimani V, Vincheh FH (2013) Improving ant colony optimization for brain MRI image segmentation and brain tumor diagnosis. In: 2013 First Iranian conference on pattern recognition and image analysis (PRIA) (pp. 1–6). IEEE
50. Jafari M, Shafaghi R (2012) A hybrid approach for automatic tumor detection of brain MRI using support vector machine and genetic algorithm. Glob J Sci, Eng Technol 3:1–8
51. Yin PY (1999) A fast scheme for optimal thresholding using genetic algorithms. Signal Process 72(2):85–95
52. Pugalenthi R, Rajakumar MP, Ramya J, Rajinikanth V (2019) Evaluation and classification of the brain tumor MRI using machine learning technique. J Control Eng Appl Inform 21(4):12–21
53. Natarajan P, Krishnan N, Kenkre NS, Nancy S, Singh BP (2012) Tumor detection using threshold operation in MRI brain images. In: 2012 IEEE International conference on computational intelligence and computing research (pp. 1–4). IEEE
54. Manogaran G, Shakeel PM, Hassanein AS, Kumar PM, Babu GC (2018) Machine learning approach-based gamma distribution for brain tumor detection and data sample imbalance analysis. IEEE Access 7:12–19
55. Havaei M, Davy A, Warde-Farley D, Biard A, Courville A, Bengio Y, Larochelle H (2017) Brain tumor segmentation with deep neural networks. Med Image Anal 35:18–31
56. Bansal P, Gupta S, Kumar S, Sharma S, Sharma S (2019) MLP-LOA: a metaheuristic approach to design an optimal multilayer perceptron. Soft Comput 23(23):12331–12345
57. Vrugt JA, Beven KJ (2018) Embracing equifinality with efficiency: limits of acceptability sampling using the DREAM (LOA) algorithm. J Hydrol 559:954–971
58. Li H, Wang D, Abreu JRC, Zhao Q, Pineda OB (2021) PSO+LOA: hybrid constrained optimization for scheduling scientific workflows in the cloud. J Supercomput 73:1–27
59. http://www.medinfo.cs.ucy.ac.cy/
60. Zhuang AH, Valentino DJ, Toga AW (2006) Skull-stripping magnetic resonance brain images using a model-based level set. Neuroimage 32(1):79–92
61. Vijh S, Sarma R, Kumar S (2021) Lung tumor segmentation using marker- controlled watershed and support vector machine. Int J E-Health Med Commun (IJEHMC) 12(2):51–64
62. Salehi H, Vahidi J, Abdeljawad T, Khan A, Rad SYB (2020) A SAR image despeckling method based on an extended adaptive wiener filter and extended guided filter. Remote Sens 12(15):2371
63. Singh A (2019) Laplacian whale optimization algorithm. Int J Syst Assur Eng Manag 10(4):713–730
64. Jain A, Zongker D (1997) Feature selection: evaluation, application, and small sample performance. IEEE Trans Pattern Anal Mach Intell 19(2):153–158
65. Malegori C, Franzetti L, Guidetti R, Casiraghi E, Rossi R (2016) GLCM, an image analysis technique for early detection of biofilm. J Food Eng 185:48–55
66. Zayed N, Elnemr HA (2015) Statistical analysis of haralick texture features to discriminate lung abnormalities. J Biomed Imaging 2015:12
67. Jiang J, Trundle P, Ren J (2010) Medical image analysis with artificial neural networks. Comput Med Imaging Graph 34(8):617–631
68. Rajini NH, Bhavani R (2011) Classification of MRI brain images using k- nearest neighbor and artificial neural network. In: 2011 International conference on recent trends in information technology (ICRTIT) (pp. 563–568). IEEE
69. Suzuki K (2017) Overview of deep learning in medical imaging. Radiol Phys Technol 10(3):257–273
70. Cheng R, Li M, Tian Y, Zhang X, Yang S, Jin Y, Yao X (2017). Benchmark functions for CEC'2017 competition on evolutionary many-objective optimization. In Proc. IEEE Congr. Evol. Comput. (pp. 1–20).
71. Hore A, Ziou D (2010). Image quality metrics: PSNR vs. SSIM. In: 2010 20th International conference on pattern recognition (pp. 2366–2369). IEEE.
72. Tanchenko A (2014) Visual-PSNR measure of image quality. J Vis Commun Image Represent 25(5):874–878